

REVIEW ABOUT COHERENT AND INCOHERENT IMAGING SIGNALS FOR COMPUTERIZED NEUTRON TOMOGRAPHY

W. Treimer^{1,2}, A. Hilger¹, N. Kardjilov¹, M. Strobl^{1,2}

¹ University of Applied Sciences (TFH) Berlin, FB II, D – 13353 Berlin, Germany

² Hahn-Meitner-Institut Berlin, SF3, D- 14109 Berlin, Germany

Abstract

In the last decade computerized neutron tomography has experienced a number of improvements which were realized by different groups, but which became not so familiar as the well known “old” signals known from radiography and tomography. So it seems to be useful to give a summary over all known neutron imaging signals that will be used nowadays and to give some examples of them. The distinction between incoherent and coherent signals appears to be helpful concerning the wide range of (possible) signals that are used for imaging and image processing. The kind of signals will be limited to the ones that have been already used in neutron tomography, so there will be no discussion about e.g. electric field tomography or impedance tomography.

Introduction

Talking about incoherent and coherent (imaging) signals one has to state what is understood by an incoherent signal or by a coherent one. From optic lectures it is well known that two (or more) points of an electromagnetic wave emerging from a point source can be seen to be coherent to each other if there is a constant phase relationship between them or if there is a given function, that describes the evolution of the phase in space or time. It is further known, that neutrons can be seen as particles and as waves because a neutron has after de Broglie a wave length $\lambda = h/p$, ($h =$ Planck’ constant, $p = mv$), and therefore the distinction between incoherent signals and coherent ones simplifies the discussion about different interactions in neutron radiography and tomography. The fundamental entity we are dealing with is the index of refraction n , given by

$$n = 1 - \delta + i\beta \quad (1)$$

with [1]

$$\delta + i\beta = \lambda^2 \frac{N}{2\pi} \sqrt{b_c^2 - \left(\frac{\sigma_t}{2\lambda}\right)^2} + i \frac{\sigma_{r^N} \cdot \lambda}{4\pi} \quad (2)$$

If $\sigma_r < 2\lambda$, δ becomes

$$\delta = \lambda^2 \frac{N b_c}{2\pi} \quad (3)$$

and

$$\beta = \frac{\sigma_{r^N}}{4\pi} \quad (4)$$

$\lambda =$ wavelength, $N =$ number of scattering centers/unit volume, $b_c =$ coherent scattering length and σ_t is the sum of the absorption cross section σ_a and the scattering cross section σ_s [2]:

$$\sigma_t = \sigma_a + \sigma_s \quad (5)$$

δ without the cross section term is responsible for the “wave character” of the neutron, because it influences the phase (and phase front) of a wave if it traverses a medium. δ or b_c respectively is determined experimentally because this quantity cannot be described by a sufficient satisfactory theory based on strong interaction. β is the part that is responsible for the attenuation (= absorption + scattering) and usually counted as the “particle” part of the index of refraction. In the absorption process of a neutron a compound nucleus is formed, that decays by α , β or γ radiation which can be measured. Because absorption is a statistical process no phase relation or interference effects are observed. However, both parts together can be given by a single term χ . The change of the phase for a given sample thickness ΔD and attenuation cross section σ_t is [3]:

$$\chi = -\lambda N \Delta D \sqrt{b_c^2 - \left[\frac{\sigma_t}{2\lambda} \right]^2} + \frac{1}{2} i \sigma_t N \Delta D \quad (6)$$

Note that both parts of equ. 6 influences the interference pattern which can be measured with a neutron interferometer. In this case the sample is located in one of two coherent beams of a (neutron) interferometer, which are brought to a coherent overlap that produces a phase modulated two-dimensional picture. To determine the absolute phase-number, several phase shifts with the sample are recorded and evaluated. From these measurements one can reconstruct phase images, which is in the case of neutron a very difficult procedure. The “wave term” shifts the phase, the “particle term” decreases the amplitude of the interfering partial waves. In the case of x-rays this technique was already realized [4], [5]. In this paper, however, we restrict the consideration on non-interferometric measurements.

Phase contrast

A wave traversing a sample passes a two-dimensional field $\delta = \delta(x,y)$ and the resultant change of the phase along this path is simply calculated with the path integral

$$\phi = \frac{2\pi}{\lambda} \int_{Path} \delta(s) ds \quad (7)$$

The same happens to the other part β of equ.(1). The amplitude of the wave decreases by the factor $e^{-2\pi i \beta}$. If $\mu = \mu(x,y)$ denotes the two-dimensional function that describes the absorption of radiation in a slice, $\mu(x,y)$ is given by

$$\mu(x, y) = -\frac{4\pi}{\lambda} \int_{Path} \beta(s) ds \quad (8)$$

The phase terms can be measured different than with an interferometer as was demonstrated some years ago [6]. In that paper it was shown, that phase based intensity variation can be observed by a rather simple technique. A cold neutron beam and a small pinhole produced Fresnel diffraction downstream of the sample, that can be imaged with a position sensitive detector at the right distance from small objects. More detailed studies were performed later and proved the feasibility of this method [7].

The idea of phase contrast imaging is the following: Consider a (neutron) wave which is coherent in a region given by the first Fresnel zone. The size of the first Fresnel zone (FZ) A_{FZ} is

$$A_{FZ} = \frac{R \cdot r}{R + r} \cdot \pi \cdot \lambda \cdot \frac{1}{\sin(\theta)} \quad (9)$$

with R = distance point source–object, r = distance object–detector and θ the angle between the ray propagation vector and the plane of observation (usually $\theta = 90^\circ$). This size A_{FZ} determines the coherent source for any interference effects. For standard geometries (e.g. $R \sim 500$ cm, $r \sim 1$ cm, $\lambda \sim 0.5$ nm) A_{FZ} is app. 1.6×10^{-7} cm² and the diameter of the coherent source ~ 4 μ m. Usually one has to create a point-like source by a small pinhole, that determines together with the divergence of the beam the size the coherent area d_{coh} of a real neutron beam. The coherent size of a source d_{coh} can also be estimated by simple geometric considerations as [8]

$$d_{coh} = \lambda \cdot \frac{1}{2} \frac{R}{D} \quad (10)$$

d_{coh} = size of the monochromatic source, R/D the common known “L/D - ratio”. A short calculation demonstrates, that D must be kept very small, of the order some hundred microns or even less, to achieve a reasonable size of the coherent “source area”. In the case of phase contrast the coherent part of the wave propagates through an object and experiences position dependent phase shifts, i.e. the propagating wave front is modulated by different indices of refractions in the sample. The modulation occurs quite rapidly in the so-called near field region ($z < d^2/\lambda$), z = distance object–detector, d = diameter of the object and it broadens with increasing z . The fringe modulation caused e.g. by an edge is washed out in the case of a too large divergence and/or source size. To observe the strongest phase contrast, one has to operate in the near field region, where $z < d^2/\lambda$, where the modulation of the

amplitude is best. It can be shown that the optimal contrast occurs at $z = d^2/2\lambda$. This was (partially) proved by the investigations of contrast images of steel needles at different detector distances and L/D [7], [9]. In the case of neutrons, most samples can be treated with this theory for (rather) weak absorbing materials, i.e. thin objects in the sense of absorption. Fig.1a and 1b show the result of an experiment, performed at the PSI (Swiss) [15] .

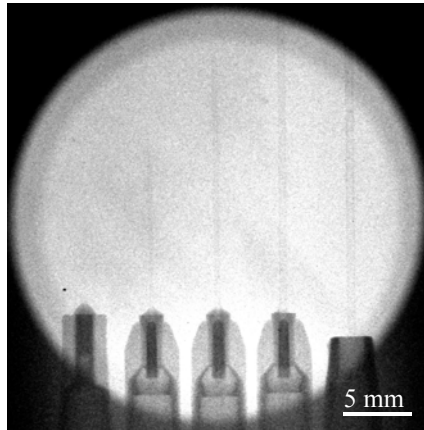


Fig. 1a Distance sample to detector: 0 cm
Distance pinhole to sample: 650 cm
Pinhole diameter: 0.5 mm
Exposure time: 180 min

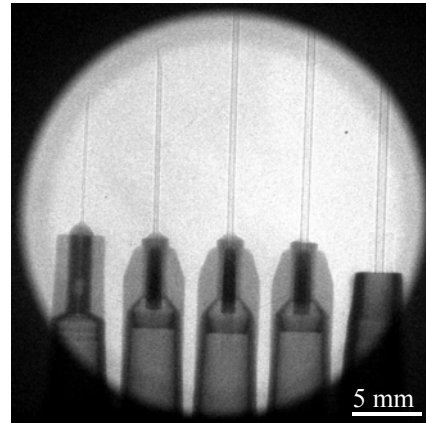


Fig. 1b Distance sample to detector: 100 cm
Distance pinhole to sample: 650 cm
Pinhole diameter: 0.5 mm
Exposure time: 180 min

Refraction and ultra small angle contrast

Another method to image phase contrast was investigated [10] using the coherence properties of neutrons. The idea was, that for $z > d^2/\lambda$ the wave front changes its direction, if the interface between two media is not perpendicular to the flight direction of the neutron. This is the usually the case, especially in a tomography, where the incident flight direction changes from 0 to 180°. So, e.g., in medium (2) it will deviate from the one in medium (1) in a sample, consisting of two different components (1) and (2), i.e. refraction occurs. Due to the extreme small interaction potential of a nucleus with neutrons, this deviation is - depending on the angle of incidence onto the interface - for neutrons and X-rays of the order of μrad and therefore not observed in conventional tomography. However this interaction contains information about the interface which can be used to image structures. Considering this interaction more closely, one has to distinguish between two cases, the one where incident coherent wave-front is larger and the other where it is smaller than interface of the object. In the case of refraction the coherent wave front is much smaller than the interface. The other case to consider is, if neutrons traverse structures that have sizes of the order or less of the coherent wave-front. In this cases, small angle scattering arises (or large angle scattering if diffraction is involved), which decreases the contrast in a conventional tomogram. Small angle scattering is a well known method in x-ray and neutron physics with a wide field of applications. Therefore it is of high interest to investigate the possibilities to use it for tomography. In the case of pure refraction interaction, a neutron or x-ray in a sample is many times deflected (zigzag path) and leaves the sample with a different flight direction compared to the one in front of the sample (Fig. 2).

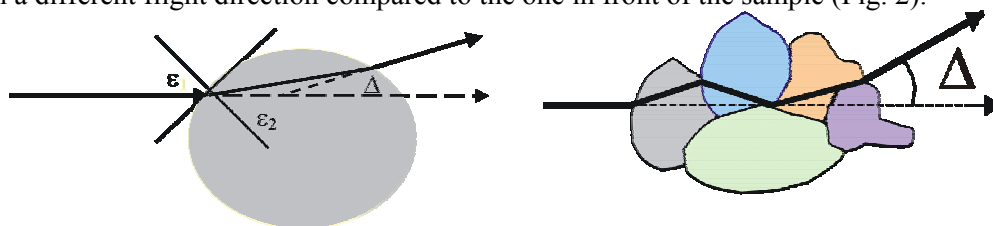


Fig.2 Refraction by an homogeneous and inhomogeneous sample. The neutron follows a zig-zag path if it traverses a sample

In the case of small angle scattering the scattering pattern (i.e. the measured intensity distribution) is broadened due to coherent scattering by structures that have sizes of the order of $\sim 10\text{nm} - 10\mu\text{m}$. For both scattering effects, refraction and small angle scattering, one can consider the path of a neutron or X-ray through a sample as a straight line, i.e. the volume of interaction does not change due to refraction or small angle scattering. This assumption can be done because the sum of all angular deviations is small as compared to the divergence of the beam. However, the integrated deviation of the flight direction from the incident direction must be determined. To apply these considerations to equations, we consider a function $n(x,y)$ that describes the position dependent index of refraction: $n(x,y) \neq 1$ inside the sample and $n(x,y) = 1$ outside. From the Snellius law one gets $n_1 \sin(\varepsilon_1) = n_2 \sin(\varepsilon_2)$, with ε_1 as the corresponding angle of incidence and ε_2 the refraction angle, n_1 and n_2 are the corresponding indices of refraction of medium (1) and medium (2). From simple geometrical optics it is also well known, that the larger ε_1 the larger is ε_2 up to the case of total reflection. Leaving the sample, the ray will have a final angle of deflection Δ , which is the sum of all individual deflections δ_i ($\delta_i = \varepsilon_i - \varepsilon_{i+1}$) along the path through the sample:

$$\Delta = \sum_{i=1}^n \xi_i \quad (1)$$

A deflection ξ_i from the preceding direction is only present at the adjacent volumes with different indices of refraction and if $\bar{k} \cdot \nabla n(x,y) \neq 0$ (\bar{k} is the neutron wave vector). One can determine Δ and by that $n(x,y)$ by measuring Δ of each path (line integral) and varying the orientation θ of the sample from 0° to 180° . If $\bar{k} = (\bar{k}_p, \bar{k}_\perp)$ is represented by a component parallel and perpendicular to $\nabla n(x,y)$, and \bar{k}_\perp is the component of \bar{k} parallel to $\nabla n(x,y)$, then a point $P_\theta(t)$ of a projection is given by

$$P_\theta(t) = P(t, \theta) = \int_{\text{Path}} \nabla n(x,y) \cdot \bar{k}_\perp ds \quad (2)$$

A simple calculation of Δ for a given orientation θ for a brass sample (cp. Fig.3, $\varnothing = 10\text{mm}$ four holes with $\varnothing = 1, 2, 3$ and 4 mm) is shown in Fig.3 .

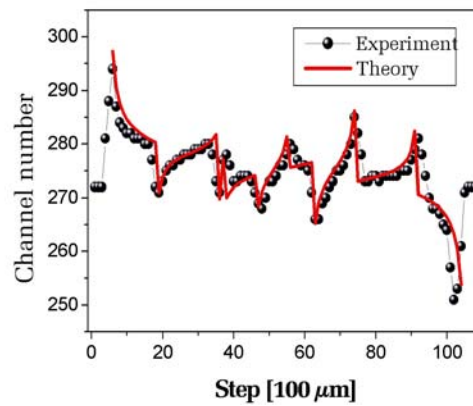


Fig.3 : Calculated and measured peak shift for a certain orientation θ of a brass sample. The channel number 272 denotes the center of the unaffected peak ($\Delta = 0$) and a single channel corresponds to 1.4 sec of arc

The measurement was done with a special double crystal diffractometer as shown in Fig.4. We used different shaped Al samples to point out the effect of refraction. The samples were placed between monochromator and analyser and scanned perpendicular to the neutron beam, the slit defines the special resolution. The analyser – together with the position sensitive detector – provides the simultaneous measurement of absorption, refraction and small angle scattering. The results are shown in Fig. 5.

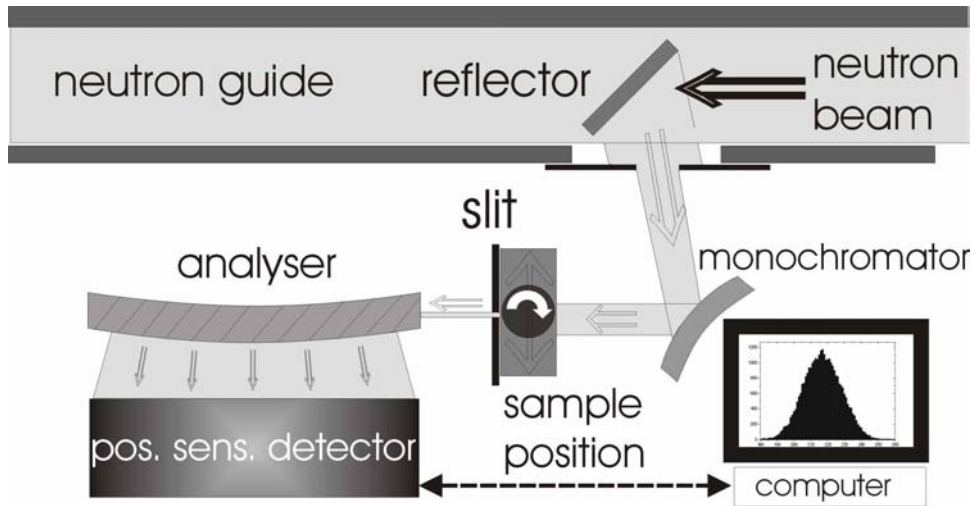


Fig.4 Set up of the double crystal diffractometer V12a at the Hahn-Meitner-Institute. Monochromator and analyser are perfect Si crystals, (111) reflection, $\lambda = 0.467$ nm.

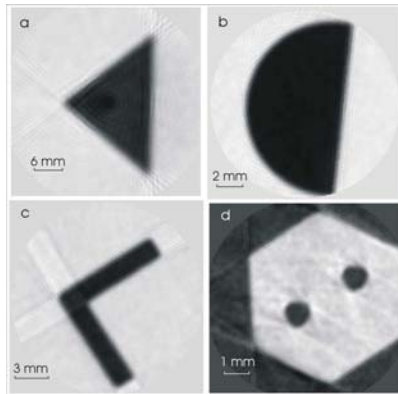


Fig.5 : Tomograms reconstructed with refraction data only. Note the artefacts if long straight areas give rise to total reflection as well.

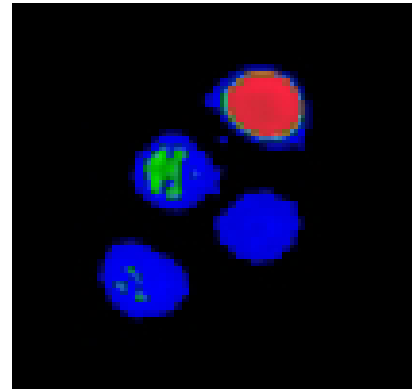


Fig.6 2D Reconstruction with pure SANS data, blue ~ 3.8 wt%, green ~ 5.8 wt% , red~ 12 wt % (~150 nm β -Carotene particles).

Recently a Al cylinder, diameter 20mm , height 30mm, holes = 3mm and 1mm, app. 20° oblique) has been three-dimensionally constructed based only on data due to refraction [11]. The advantages of this technique are apparent, no dependence on the size of a monochromatic source, no limit for the size of the objects under investigation, the disadvantage is the low available neutron flux in a double crystal diffractometer, because one has to use monochromatic neutrons and therefore long exposure times (hours - days).

Using a double crystal diffractometer, as shown in Fig.4, one also can reconstruct density variation due to small angle scattering of e.g. particles of the size of a few hundred nanometer [12]. If the lateral coherent length is larger than the structure, one observes small – or ultra small angle scattering, depending on the size of the structures that cause scattering. The broadening can be calculated for thick samples as [13]

$$B = \sqrt{\int_{Path} \frac{\sigma(x,y) \cdot N(x,y)}{R(x,y)^2} ds} \quad (3)$$

with $\sigma(x,y)$ = scattering cross section, $N(x,y)$ = density of the scattering particles and $R(x,y)$ is a parameter specifying the correlation length, i.e. the average size of the scattering particles at (x,y) . For a constant particle size, R is therefore is inverse proportionally to B . B becomes then a measure for the particle density for a given $\sigma(x,y)$. The projection function $P_\theta(t)$ (i.e. the measured logarithmic intensity of a projection) is then proportionally to B^2 which can be reconstructed with standard methods [14].

With this method density variations between 5% and 12% of 150 nm particles of β – carotene in D_2O could be two-dimensionally reconstructed [12] (Fig. 6).

Incoherent signals

Energy dependent radiography and tomography

Incoherent imaging signals for neutron radiography and tomography are all based on absorption. However, different techniques such as energy – dependent computerized tomography or real time tomography open a wide ranging field of applications. Beside radiography and conventional tomography these methods have gained an increasing interest. This comes from several physical problems that have to be solved, and from the possibility to use some special features of absorption plus a cold neutron spectrum. For the energy disperse radiography and tomography the behavior of the absorption cross section is the important entity. For cold neutrons the cross section dependency on the energy is shown in Fig.7 for Fe:

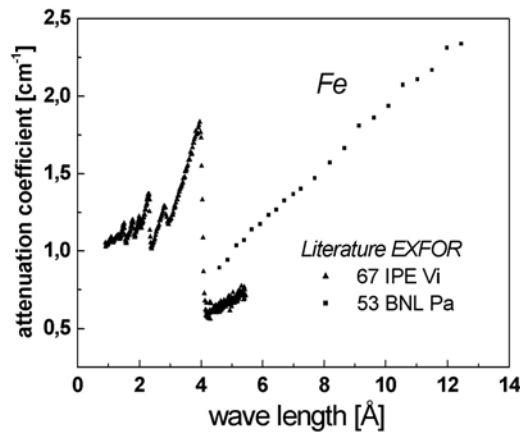


Fig.7 Wave length dependency of the attenuation coefficient for Fe.

One recognizes a sharp edge close to 4 Å (absorption edge) which can be used for selective tomography. The different amount of the attenuation for different wave length gives an intensity ratio as

$$\frac{\frac{I_1}{I_{01}}}{\frac{I_2}{I_{02}}} = \frac{I_1 \cdot I_{02}}{I_2 \cdot I_{01}} = \frac{e^{-\Sigma(\lambda_1)d}}{e^{-\Sigma(\lambda_2)d}} = e^{[\Sigma(\lambda_2) - \Sigma(\lambda_1)]d} \quad (4)$$

A radiogram (or tomogram) taken at two different wave lengths enables one to enhance or suppress details in the picture as can be seen in Fig.8 [15]

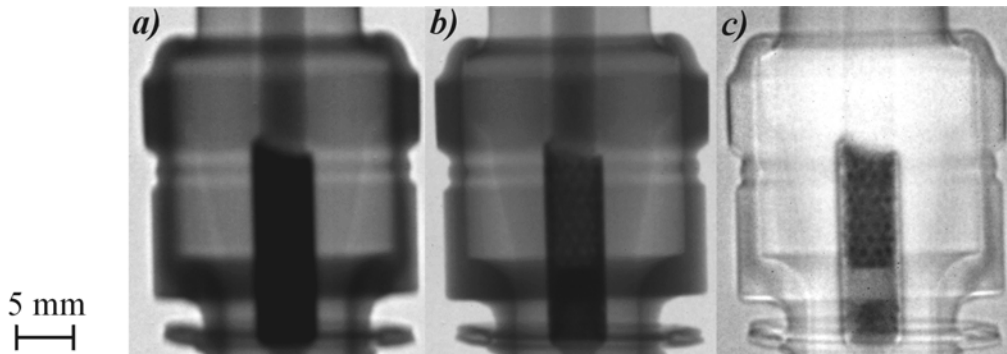
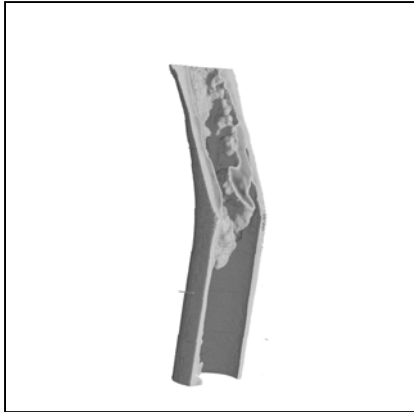


Fig.8 Radiographs of a spark plug at 6.9Å (a) and 3.2Å (b). The division of both images (c).



However, sometimes it is better to use monochromatic neutrons rather than the full spectrum. Recent experiments to visualize oil and carbon deposits in tubes by means of neutron tomography (Fig.9) have proved, that sometimes less flux, but monochromatic neutrons deliver sometimes better results, but without activating the sample which is a problem for high flux neutron CT. With a full wave length spectrum (and much more neutrons) less details can be imaged due to λ – smearing and beam hardening.

Fig. 9 Part of a tube which has with carbon and oil deposits.

Real time radiography and tomography

Finally some remarks should be made to real time tomography. Real time tomography offers the possibility to visualize rapid processes in e.g. automobile industry, combustion processes, etc., in hydrodynamics, water flows (with D_2O), stress and strain developments, but also in biology and other fields of science. For technicians and theoreticians it is important to compare computer simulations with real experimental data, to improve the theory or a mechanical solution of a problem. However, real time radiography or tomography can be done only at high flux beam lines with neutron fluxes more than at least 10^7 n/cm².sec.

To visualize rapid processes one has to distinguish between oscillating and simple emerging (non-oscillating) processes. In the latter case each shot (or frame) must be able to image (by absorption) within a certain time interval Δt an instantaneous progress of the process. The process itself can be visualized by registering as many frames as possible. In the case of oscillating movements – as is was

done in Fig. 10 – the motion was triggered, so that different portions of the piston could be imaged at different times. The sharpness of the pictures and therefore of the film depends on the number of neutrons which can be collected within one pixel (Δx) within Δt (per frame) and how well defined the triggering can be managed. Therefore the exposure time Δt should be smaller than the velocity of the process within a certain Δx ($x + \Delta x$), i.e. any detail of the oscillation process should move less than half of a pixel within the exposure time Δt .

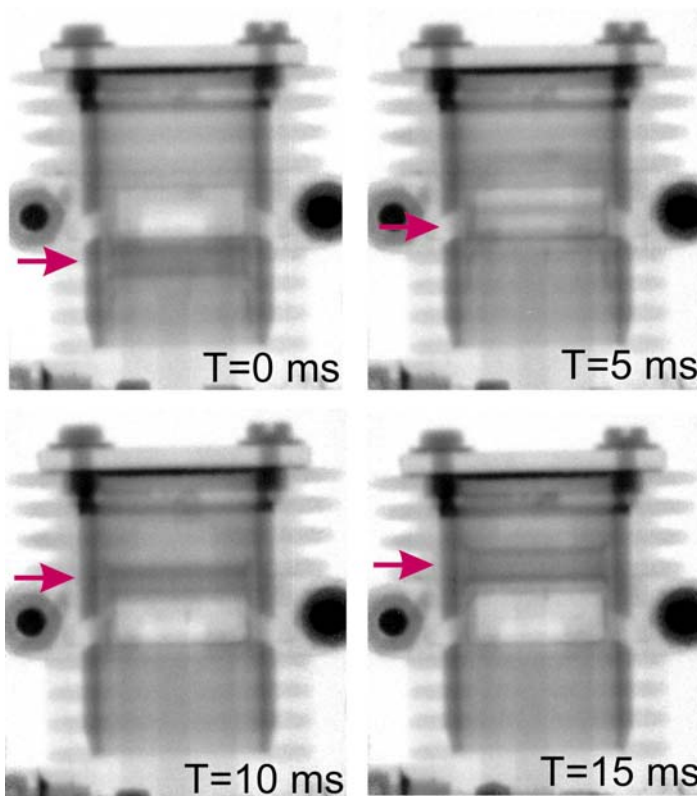


Fig. 10 Visualization of the movement of a piston of a small model aircraft machine. The motor ran with app. 1100 rpm, the exposure time was 1msec, 200 frames were added for each picture. A short film could be produced which shows the movement of the piston in slow motion.

Conclusions

The two main imaging signals – absorption and phase – the incoherent and coherent parts of the wave are the basis for high resolving imaging techniques, which become more and more sophisticated. The application of either coherent or incoherent signals depends on the problem that has to be solved, the field of applications is increasing. Non-destructive testing by means of neutron tomography has become more and more an important tool for many new technologies, which can learn from a scientific visualization of their products. Other, new imaging signals such as Fourier-CT or CT with polarized neutrons will be exploited for industrial as well as for scientific research and increase the potentials of neutron radiography and neutron tomography.

This work is part of the BMBF project 03 TR9B6

References

- [1] M.L. Goldberger and Seitz F. (1947) Phys. Rev. **71**, 294
- [2] Sometimes it is written as the reaction cross section σ_r , σ actually contains other cross section which for our purpose are rather negligible.
- [3] J. Summhammer, H. Rauch, D. Tuppinger Phys. Rev. A **36**, 9, 4447-4455 (1987)
- [4] A. Momose, T. Takeda, Y. Itai Rev. Sci. Instrum. **66** 1434 – 1436 (1995)
- [5] . Bonse, F. Beckmann, F. Busch, O. Günnewig „X-ray Microscopy and Spectromicroscopy” ed. J. Thieme, G. Schmahl, E. Umbach & D. Rudolph, Berlin-Heidelberg Springer –Verlag
- [6] B. E. Allman, P. J. McMahon, K. A. Nugent, D. Paganin, D. L. Jacobson, M. Arif, and S. A. Werner, Nature (London) **408**, 158 (2000).
- [7] See for example N. Kardjilov, E. Lehmann, E. Steichele, P. Vontobel Nucl. Instr. & Methods in Physics Research A (in print)
- [8] X. Wu, H. Liu Med. Phys. **30** (8), August (2003) state $\sim d_{coh} = 2 \cdot \lambda \cdot \frac{R}{D}$
- [9] A. Pogany, D. Gao, S. W. Wilkins Rev. Sci. Instrum. **68** (7), July 1997
- [10] W. Treimer, M. Strobl, A. Hilger, C. Seifert, U. Feye-Treimer Appl. Phys. Lett., **83**, 2 (2003)
- [11] M. Strobl, W. Treimer, A. Hilger Nucl. Instr. & Meth. accepted
- [12] W. Treimer, M. Strobl, A. Hilger, Appl. Phys. Lett. submitted
- [13] T.M. Sabine, W. K. Bertram Acta Cryst. **A55**, p 500 – 507 (1999)
- [14] M. Strobl Dissertation 2003 , University of Vienna
- [15] N. Kardjilov, S. Baechler, M. Bastürk, M. Dierick, J. Jolie, E. Lehmann, T. Materna, B. Schillinger, P. Vontobel, New features in cold neutron radiography and tomography Part I: Applied energy-selective neutron radiography and tomography, Nuclear Instruments and Methods in Physics Research A **501** (2003), 536–546